Desalination and Water Treatment
www.deswater.com
doi: 10.5004/dwt.2023.29221

283 (2023) 79–96
January

Effect of flow field and electric field coupling on oil–water emulsion separation

Zhihua Wang[a,*], Xiangdong Qi[a], Yongtao Zhuang[b], Qun Wang[a,c], Xitong Sun[a,d]

[a]*Key Laboratory for Enhanced Oil & Gas Recovery of the Ministry of Education, Northeast Petroleum University, Daqing 163318, China, emails: zhihua_wang@126.com (Z. Wang), nepuqxd@163.com (X. Qi), 704655212@qq.com (Q. Wang), 15843257944@163.com (X. Sun)*
[b]*Engineering Technology and Supervision Department, PetroChina Dagang Oilfield Company, Tianjin 300280, China, email: zhuangytao@petrochina.com.cn (Y. Zhuang)*
[c]*Oil Recovery Plant No. 3, PetroChina Daqing Oilfield Company Limited, Daqing 163113, China*
[d]*Jilin Branch of China Aviation Fuel Company Limited, Changchun 130500, China*

Received 29 July 2022; Accepted 12 December 2022

ABSTRACT

The formation and treatment of oil–water emulsion during production and transportation is intractable challenge for the oil industry. A typical process of electric field dehydration plays an active role in the separation of oil–water emulsions. However, the flowing emulsion has flow field characteristics within the electric dehydrator, and the effect of emulsion under the coupling effect of flow field and electric field has not been fully understood. In this study, a set of numerical simulation and laboratory experiments were used to show the relationship between flow field and electric field. According to the treatment process of a block in Daqing Oilfield, the model of electric dehydrator with equal proportion to the field was established, and the electric field condition was realized by user-defined function (UDF). The separation characteristics of oil–water emulsion under the effect of electric field type, intensity, frequency, and duration time were investigated by numerical simulation. The results showed that the water content at the oil outlet was lower than 1.5% and the separation rate of emulsified water was higher than 90% after a square wave electric field with intensity of 2.0 kV/cm and frequency of 3 kHz for a duration time of 20 min. The results of laboratory experiments using the bottle test method are in general agreement with the simulation results. This study is helpful to understand the coupling effect of flow field and electric field in oil–water emulsion separation process, and the results are expected to promote the development of electric field dehydration in oilfields.

Keywords: Flow field; Electric field; Coupling effect; Oil–water emulsion; Wastewater treatment

1. Introduction

Most oilfields exploit reservoirs by water injection, which makes the produced fluid contain a higher amount of water and mechanical impurities [1]. Therefore, oil–water separation has always been an important work in crude oil treatment [2,3]. Furthermore, the water content of the produced water is increasing during the continuous development of the oilfield, and the development mode is changing to diversification, such as polymer flooding, alkaline/surfactant/polymer flooding, gas flooding, etc. which means that the properties of produced water become more complex, and the difficulty of oil–water separation is further increased [4–9]. Free water in crude oil can be removed by gravity sedimentation in a short time [10,11]. However, some water is agitated and sheared in the flow and mixed with crude oil to form oil–water emulsion in the presence of emulsifier [12]. Their removal is much more difficult than free water. Asphaltenes,

* Corresponding author.

colloids and waxes in crude oil are natural emulsifiers [13]. In addition, in order to enhanced oil recovery efficiency, chemical flooding agents added artificially in the process of oil recovery will also play the role of emulsifiers, thus the stability of oil–water emulsion is further strengthened, and oil–water separation is challenged [6,9,12,14].

In the above context, a number of methods for separating oil–water emulsions have emerged, including chemistry, centrifugation, heating, machinery, and electric field [15]. For example, Pramadika et al. [16] found that the use of sulfuric acid demulsification can greatly improve the efficiency of oil–water emulsion membrane separation. Gong et al. [17] proposed an electric field enhanced swirling centrifugation separation device, which can simultaneously use the coupling effect of centrifugal field and electric field to achieve rapid separation of oil and water. Abdurahman et al. [18] used microwave heating for demulsification and no chemical demulsifier was added throughout the process. Solovyev et al. [19] studied the mechanical structure of the emulsion separator and proposed that optimum baffle inclination angle was 65°. Atehortúa et al. [20] introduced ultrasonic standing wave field to separate oil–water emulsion, and the separation effect was better than gravity conditions. Li et al. [21] prepared an air superhydrophilic/superoleophobic diatomite porous ceramics for efficient separation of oil–water emulsions. Li et al. [22] used the high-voltage electric field in the triboelectric dehydrator to make the dehydration rate of oil–water emulsion with water cut of 60% reach 99.41%. Ren and Kang [23] studied the separation of oil–water emulsions under a bidirectional pulsed electric field and further demonstrated the microscopic aggregation effect of oil droplets in emulsion. Esmaelion et al. [24] evaluated the adaptability of nanofibers filter to separate oil–water emulsions. The dehydration effect of demulsifier and pulsed electric field s were investigated, and further proposed their synergistic effect [25]. The dehydration effect under the coupling of electric field and magnetic field is described by Guo et al. [26], and the optimal collocation of AC electric field and steady magnetic field is obtained.

In general, electric field dehydration with electric dehydrator as the main equipment has the advantages of large treatment capacity and good treatment effect, and has been widely used in oilfields and refineries. The demulsification process of oil–water emulsion in electric field has been clearly described, and the coalescence mechanism of water droplets through electrophoresis, dipole and oscillating coalescence in electric field has been well revealed [27–33]. However, in the treatment process of oil fields or refineries, the oil–water emulsion in the electric dehydrator is in a flow state, which determines that the dehydration process will be affected by the coupling effect of flow field and electric field. Therefore, the flow field characteristics of emulsified water separation under the action of electric field are further described, especially the effect of oil–water emulsion under the coupling effect of flow field and electric field, which is of great significance to the optimal operation of electric field dehydration.

In this study, the model of the vertical electrode plate electric dehydrator in equal proportion to the field was established, and the UDF was written to introduce the electric field condition. The EULERIAN model and the RNG k–ε model were applied. The separation characteristics of emulsions under the effect of electric field type, intensity, current frequency, and duration time were studied by numerical simulation. By observing the internal pressure field, streamline characteristics, and oil phase volume fraction distribution of the dehydrator, the separation characteristics and effect of emulsions under the coupling effect of flow field and electric field were described by the combination of qualitative and quantitative methods. The optimal operation parameters of electric field dehydration were obtained, and the simulation was verified by corresponding experiments.

2. Methodology

2.1. Experiments

2.1.1. Experimental materials

The materials for preparing oil–water emulsion were taken from a block in Daqing Oilfield. The freezing point of crude oil was 28.7°C, and the contents of wax, colloid and asphaltene were 23.2%, 9.50% and 1.60%. The polymer added to the emulsion is anionic partially hydrolyzed polyacrylamide with a molecular weight of 1.9×10^7. The demulsifier used in the electric field dehydration is alkyl phenolic resin water–soluble demulsifier. The experimental instruments were the high shear emulsification machine, the crude oil dehydration performance tester, the electric field dehydration tester, and the ultraviolet-visible spectrophotometer. The construction of different electric fields can be realized by the electric field dehydration tester.

2.1.2. Experimental procedure

As shown in Fig. 1a, a high shear emulsification machine was employed to prepare emulsion. The mechanical and hydraulic shearing of oil–water emulsion is realized through the precise coordination of rotor and stator during rotation, so as to achieve the purpose of dispersion and emulsification. Moreover, thermostatic heating plate can meet the temperature control of oil and water medium in the mixing cylinder. The electric field dehydration tester mainly consists of a high-voltage rectifier module, a temperature control module and a programmable controller, as shown in Fig. 1b, an electric field is constructed in the bottles connected to the high-voltage rectifier module. After an effective electric field is applied, the water droplets in the emulsion are polarized and vibrate periodically. The strong electrostatic force between the water droplets promotes collision and agglomeration, the dipole force promotes stretching deformation, and the interfacial tension promotes shape recovery, thus achieving the separation of emulsified water in reciprocal, periodic stretching vibration.

In the experiment, an appropriate amount of crude oil and water are taken to prepare emulsion with different water content and then the high shear emulsion machine (Φ3 mm mesh stator head) was used to continuously shear for 2 min at the speed of 6,000 rpm [34,35]. The water content of the emulsions obtained after preparation was 50%, 65% and 85% at a polymer concentration of 1,000 mg/L. Next, the

free water sedimentation separation experiment was carried out for oily sewage, and the sedimentation separation temperature was 40°C and time was 120 min. Then the demulsifier was added to the oil–water emulsion obtained after sedimentation separation, and the dosage was 120 mg/L. The electric field dehydration was carried out according to the experimental scheme, and the dehydration temperature was controlled at 60°C.

2.1.3. Experimental scheme

The experiment simulates the produced emulsion treatment process in Daqing Oilfield. The free water is removed before the electric field dehydration of oil–water emulsion. The effect of electric field type, intensity and duration time on the electric field separation of emulsified water was tested by bottle test method. The experimental scheme as shown in Table 1.

2.2. Numerical simulations

2.2.1. Building physical models

The physical model of vertical electrode plate electric dehydrator is established, and the specification is Φ2,620 mm × 9,333 mm. Because the emulsion droplets are moved, collided, and merged in the electrode plate area under the action of electric field force, and then the separation is realized. Therefore, the device was reasonably simplified in conjunction with the need for numerical simulations. The wiring insulation rod, suspension insulator, transparent hole, population, sand discharge hole and other components are omitted. Auxiliary facilities such as safety valve, vent valve, pre-settlement chamber, oil distribution hole, oil–water interface measuring instrument, vortex breaking plate and drainage chamber are omitted. The physical model of the electric dehydrator is obtained as shown in Fig. 2. The geometric parameters of electric dehydrator are shown in Table 2.

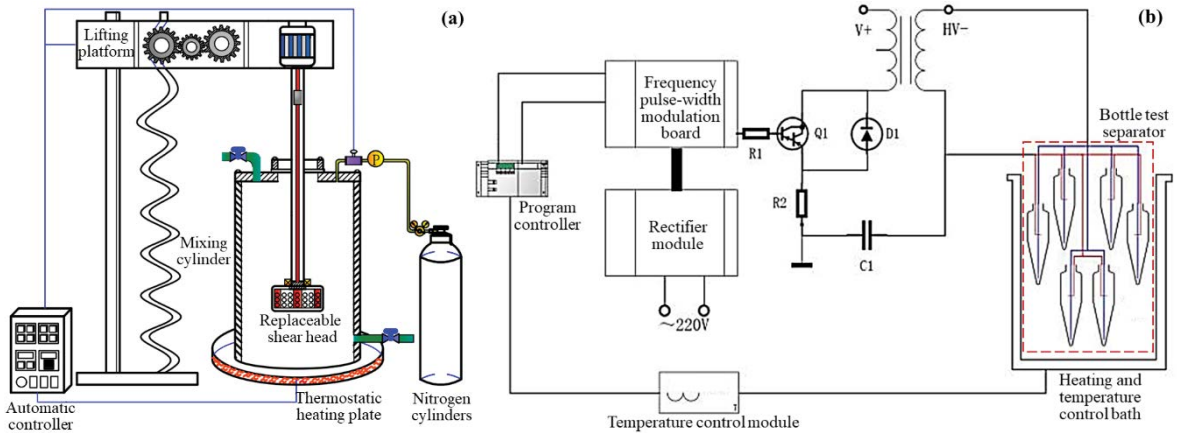

Fig. 1. Schematic of the experimental set-up with: (a) high shear emulsification machine and (b) electric field dehydration tester.

Table 1
Laboratory experiment scheme

Electric field type	Electric field intensity (kV/cm)	Current frequency (kHz)	Duration time (min)
DC electric field	1.5	–	10
			15
			20
			25
	2.0		10
			15
			20
			25
	2.5		10
			15
			20
			25
Square wave electric field	2.0	1	15
		2	
		3	
		4	

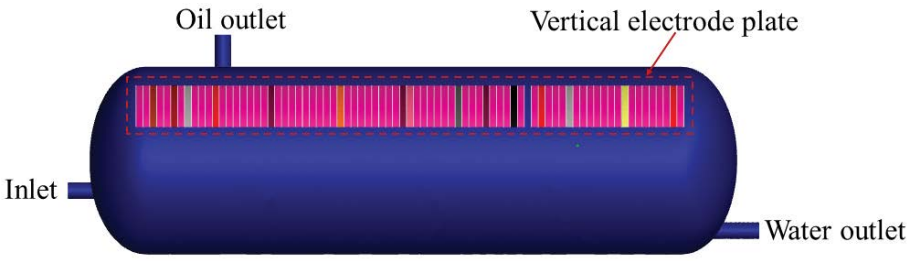

Fig. 2. Simplified physical model of electric dehydrator.

Table 2
Structural size of electric dehydrator

Structural parameter	Size	Structural parameter	Size
Total volume of dehydrator (m^3)	50	Oil outlet diameter (mm)	240
Length of straight line segment of dehydrator (mm)	7,728	Water outlet diameter (mm)	240
Inlet diameter (mm)	240	Height of vertical electrode plate (mm)	1,834
Number of vertical electrode plate (branches)	80	Length of vertical electrode plate (mm)	600
Spacing of vertical electrode plate (mm)	90	Thickness of vertical electrode plate (mm)	10

2.2.2. Using mathematical models

Due to the complexity of the flow field in the dehydrator in the process of electric field dehydration, RNG *k*–ε Turbulence Model suitable for high strain rate and large streamline curvature is selected in the study [36]. For the temperature and pressure characteristics of the electric dehydrator, the energy exchange can be ignored, and the EULERIAN Model considering the interphase force in the separation process is selected in the multiphase flow model [37,38].

Continuity equation [39].

$$\frac{\partial \rho}{\partial t}+\frac{\partial\left(\rho u_x\right)}{\partial x}+\frac{\partial\left(\rho u_y\right)}{\partial y}+\frac{\partial\left(\rho u_z\right)}{\partial z}=0 \tag{1}$$

Momentum equation [40].

$$\frac{\partial\left(\rho_m v_m\right)}{\partial t}+\nabla\left(\rho_m v_m v_m\right)=-\nabla p+\nabla\left[\mu_m\left(\nabla v_m+\nabla v_m^T\right)\right]+\rho_m g+F+\nabla\left(\sum_{k=1}^{2}\alpha_k\rho_k v_{\mathrm{dr},k} v_{\mathrm{dr},k}\right) \tag{2}$$

$$\mu_m=\sum_{k=1}^{n}\alpha_k\mu_k \tag{3}$$

$$v_{\mathrm{dr},k}=v_k-v_m \tag{4}$$

where F is the mass force, N; $v_{\mathrm{dr},k}$ is the drift velocity of phase k, m/s; v_k is the mass velocity of phase k, m/s; v_m is the mass average velocity of the mixture, m/s; α_k is the volume fraction of phase k, %; μ_k is the dynamic viscosity of phase k, Pa·s; μ_m is the dynamic viscosity of the mixed fluid, Pa·s; ρ_m is the density of the mixture, kg/m^3; ρ_k is the density of phase k, kg/m^3.

From the continuous equation of oil phase, the volume fraction equation of oil phase p can be obtained:

$$\frac{\partial\left(\alpha_p\rho_p\right)}{\partial t}+\nabla\left(\alpha_p\rho_p v_m\right)=-\nabla\left(\alpha_p\rho_p v_{\mathrm{dr},p}\right) \tag{5}$$

where $v_{\mathrm{dr},p}$ is the drift velocity of phase p, m/s; α_p is the volume fraction of phase p, %; ρ_p is the density of phase p, kg/m^3.

The transport equations for the RNG *k*–ε Model [36].

$$\frac{\partial\left(\rho k\right)}{\partial t}+\frac{\partial\left(\rho k u_i\right)}{\partial x_i}=\frac{\partial}{\partial x_j}\left[\left(\alpha_k u_{\mathrm{eff}}\right)\frac{\partial k}{\partial x_i}\right]+G_k+G_b-\rho\varepsilon-Y_M+S_K \tag{6}$$

where ρ is the density of the mixture, kg/m^3; u is the velocity of the incoming fluid in the x-direction, m/s; G_k represents the turbulent energy due to the mean velocity gradient; G_b is the turbulent energy due to the buoyancy effect; Y_M is the effect of impulse expansion on the dissipation rate in compressible turbulence; S_k is a custom source item.

The electric field equation:

$$E=\frac{U}{d} \tag{7}$$

where E is the electric field strength, kV/cm; U is the electrical potential difference, V; d is the pitch of the electrode plate, cm.

2.2.3. Computational details

The unstructured polyhedron mesh is generated by Fluent Meshing. Because the reconstruction of flow field

characteristics and the analysis of emulsion separation effect need to focus on the vertical electrode plate area, therefore, in the process of unstructured polyhedron mesh generation, the electrode plate area mesh is moderately encrypted. Furthermore, the changes in parameters are also evaluated by increasing the number of mesh in the computational domain. The domain is meshed with four different meshes, from coarse to fine, are considered, the total mesh numbers are 2,987,351; 5,062,435; 5,840,110 and 7,206,448. As represented in Fig. 3, mesh convergence tests show that the difference between the pressure drop at the oil outlet and the water outlet stays below 5% as the number of grids increases. Therefore, a total of 5,840,110 polyhedra are placed in the computational domain, as shown in Fig. 4.

Based on the simplified physical model, it is assumed that the oil–water emulsion is a mixture of oil and water, and its density changes little during the separation process, so it is an incompressible fluid. In addition, the temperature of the whole separation process is constant, and the electric field between the vertical electrodes of the electric dehydrator is uniform. The simulation parameters of emulsion separation in electric dehydrator are determined according to the actual situation of Daqing Oilfield, as shown in Table 3.

The effect of viscosity at the wall boundary towards the electric dehydrator is considered, and the wall of model is set to "Standard Wall". The inlet boundary is set to "Velocity Inlet" and the outlet boundary is set to "Outflow". The unsteady calculation method is selected, and the phase coupled SIMPLE algorithm is used for the solution setting. The gradient is selected based on the Least Squares Cell Based of the cell. The momentum and volume fraction interpolation schemes are selected as QUICK schemes, and the pressure interpolation scheme is selected as PRESTO! For the discretization of the time term, the first-order implicit scheme is adopted. Under the premise of ensuring the calculation accuracy, the relaxation factor of each variable is selected as "Default". Moreover, the function of constructing electric field is not included by FLUENT software. Therefore, the construction of electric field is realized by using the UDF written in Appendix.

3. Results and discussion

In the electric dehydration process, the separation characteristics of oil–water emulsion under the coupling of flow field and electric field are related to the internal pressure, oil and water phase volume fraction, velocity and streamline trajectory of the electric dehydrator. Therefore, in the process of emulsion electric dehydration, the evolution

Table 3
Basic parameters of simulation calculation

Parameters	Value
Water phase density (kg/m^3)	1,000
Polymer concentration in water phase (mg/L)	500
Oil phase density (kg/m^3)	845
Oil phase viscosity (mPa s)	25
Surface tension of oil–water two phases (N/m)	0.03
Separation temperature (°C)	60
Initial oil–water interface height (m)	0.5
Water droplet charge quantity (C)	0.02
Water cut of emulsion (%)	15

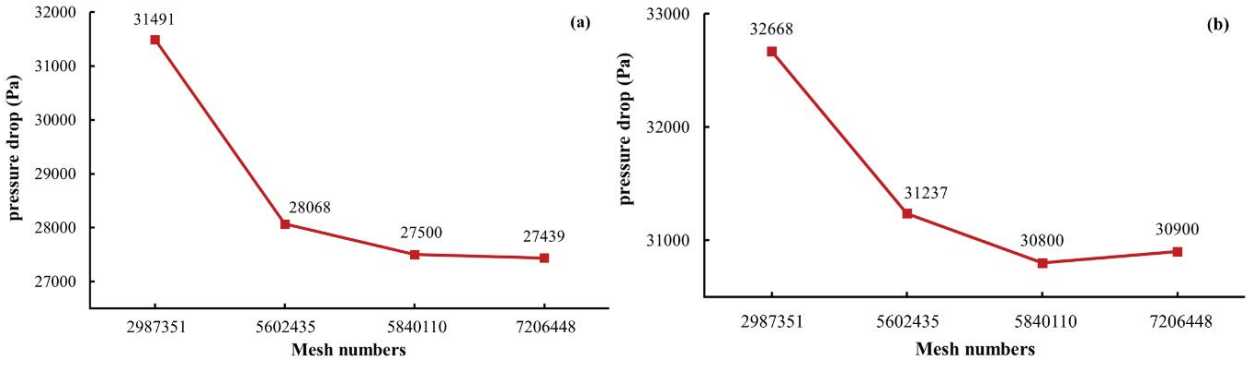

Fig. 3. Comparison of different mesh conditions with: (a) pressure drop at the oil outlet and (b) pressure drop at the water outlet.

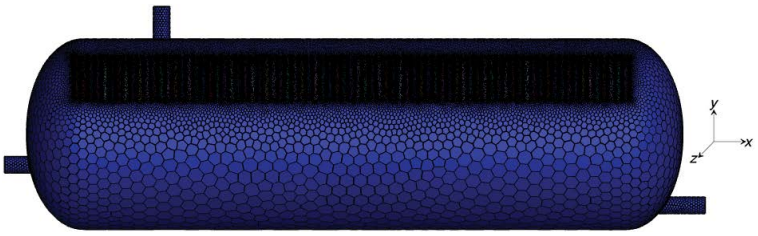

Fig. 4. Mesh subdivision of electric dehydrator.

characteristics and separation effect of flow field of electric dehydrator are described and evaluated by pressure field, oil phase volume fraction and streamline characteristics. In order to better reflect the separation characteristics of emulsion under the coupling of flow field and electric field, all the pressure field distribution and oil phase volume distribution are observed in the $Z = 0$ section, and relative to the outlet boundary, the data are extracted at the position parallel to the electric dehydrator section (y = 0.1, 0.2, 0.3, 0.4, …).

In addition, the volume fraction of oil phase and water phase at the outlet of the electric dehydrator model is extracted after calculating the stable operation, and the separation rate of emulsion is calculated according to Eq. (8) to quantitatively characterize the oil–water separation effect.

$$\eta = \frac{\varphi_{inletwater} - \varphi_{outletwater}}{\varphi_{inletwater}} \quad (8)$$

where η is separation rate of emulsion, $\phi_{inletwater}$ is volume fraction of water phase in emulsion inlet, $\phi_{outletwater}$ is volume fraction of water phase in oil outlet.

3.1. Effect of electric field types

Under the fixed conditions of electric field intensity of 1.5 kV/cm, duration time of 15 min and current frequency of 3 kHz, the UDF is loaded to simulate the typical DC field and the widely used square wave electric field, sine wave electric field and triangular wave electric field.

3.1.1. Pressure field and pressure drop characteristics

The pressure field distribution inside the dehydrator under the action of different types of electric fields is shown in Fig. 5. In the process of emulsion separation, the distribution of the four electric fields in the cross-sectional pressure drop of the dehydrator is basically the same. Compared with the outlet boundary, the cross-sectional pressure drop of square wave pulse electric field is slightly larger than that of the other three kinds of electric field types, which is attributed to the aggregation of emulsion droplets in the electrode plate under the action of electric field force. Under the coupling effect of flow field and electric field, the water phase is easy to settle, and the liquid column pressure at the bottom of the cavity increases, showing a trend of increasing cross-sectional pressure drop. The pressure drop is extracted and the curve is plotted using the average value of its cross-section. The cross-section pressure drop distribution in Fig. 6 is relatively regular. When the longitudinal position is below 1.0 m and above 2.1 m, the pressure drop of the square wave electric field is greater than that of the other three electric fields. When the longitudinal position is above 1.0 m and below 2.1 m, the characteristic curves of the pressure drop of the four electric fields are approximately coincident.

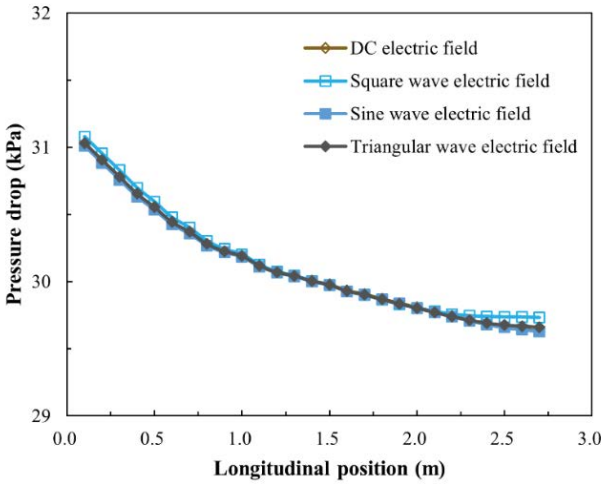

Fig. 6. Cross-sectional pressure drop characteristics of dehydrators with different electric fields.

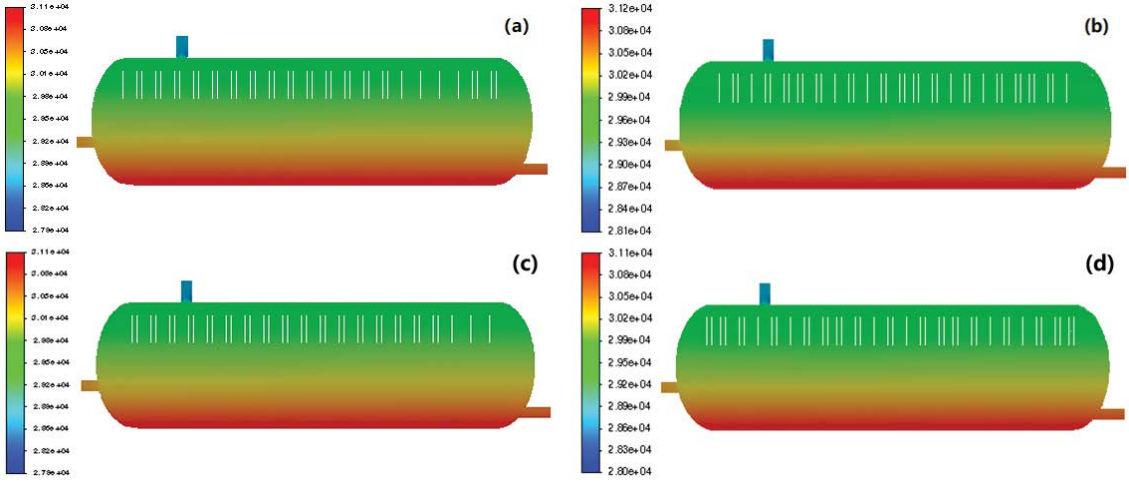

Fig. 5. Internal pressure distribution of dehydrator under electric field with: (a) DC, (b) square wave, (c) sine wave and (d) triangular wave.

3.1.2. Streamline characteristics

The flow field inside the electric dehydrator under different electric fields can be further revealed by the flow traces. As shown in Fig. 7, compared with other electric fields, under the condition of square wave electric field, the occurrence of flow field "Eddy Current" can be significantly alleviated, which is beneficial to provide a more stable separation flow field environment for its cavity.

3.1.3. Volume fraction of oil phase

The volume fraction distribution of oil phase is one of the important indexes to evaluate the separation effect of emulsion. In order to analyze the evolution process of oil–water interface and the oil phase concentration distribution in the cross-section under the action of four electric fields, the oil phase concentration distribution nephograms in the electric dehydrator under different electric fields are established. As shown in Fig. 8, the four electric fields introduced can make the dehydrator build a relatively flat oil–water interface. However, for the distribution characteristics of oil phase concentration, it can be seen that the high oil phase concentration area is thicker under the square wave electric field type, while the low oil phase concentration area is thinner.

Similarly, the proportion of oil phase volume on the cross-section of the electric dehydrator after emulsion separation under different electric fields is quantitatively analyzed, and the corresponding values are extracted. The distribution curve of the proportion of oil phase volume is plotted as shown in Fig. 9. It can be found that there is no significant difference in the proportion of average oil phase volume when the longitudinal position is less than 1.8 m, when the longitudinal position is more than 1.8 m, the average oil phase volume proportion is the highest when the square wave electric field is used.

3.1.4. Evaluation of oil–water emulsion separation effect

The effect of oil–water emulsion separation under different electric fields calculated according to Eq. (8) is shown

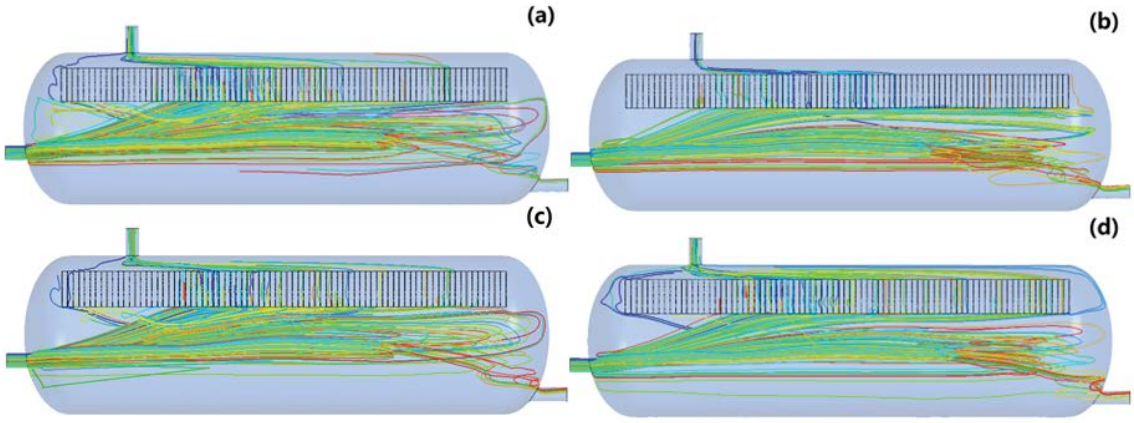

Fig. 7. Internal streamline distribution of dehydrator under electric field with: (a) DC, (b) square wave, (c) sine wave and (d) triangular wave.

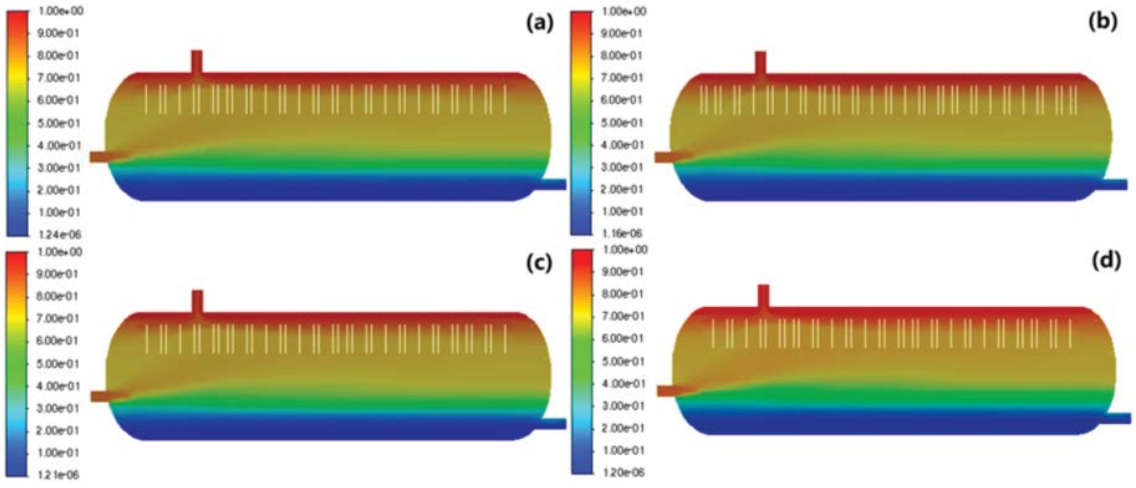

Fig. 8. Distribution of oil phase concentration proportion in dehydrator under electric field with: (a) DC, (b) square wave, (c) sine wave and (d) triangular wave.

in Table 4. In the DC electric field, the water content of oil outlet is the highest, which is 2.78%, and the corresponding separation rate of emulsified water is the lowest, which is 81.47%. In the square wave electric field, the water content of oil outlet is the lowest, which is 1.82%, and the corresponding separation rate of emulsion reaches 87.87%. It reveals that the coupling effect of square wave pulse electric field and separation flow field is more obvious to improve the separation effect of emulsion.

3.2. Effect of electric field intensity

Based on the analysis of the influence of electric field type, the electric field is reconstructed by reloading UDF. For square wave electric field, the effect of electric field intensity change on the electric dehydration effect is simulated. The control variable method is used to simulate the electric field intensity of 0.5, 1.0, 1.5, 2.0, and 2.5 kV/cm under the condition of duration time of 15 min and current frequency of 3 kHz.

3.2.1. Pressure field and pressure drop characteristics

As shown in Fig. 10, the internal pressure field distribution of the dehydrator under different electric field intensities is similar. However, when the electric field intensity increases from 0.5 to 2.5 kV/cm, although the pressure field distribution of the dehydrator is still stable, the cross-sectional pressure drop slightly increases, which is mainly due to the increase of the electric field intensity, the increase of the electric field force of the emulsified water droplets between the electrode plates, the water phase settlement separation is accelerated, and the liquid column pressure at the bottom of the dehydrator cavity is increased, showing an increase in the cross-sectional pressure drop relative to the outlet boundary. As shown in Fig. 11, the average value of the pressure drop of each section is quantitatively extracted to draw the pressure drop characteristic curve. It can be seen that the overall pressure drop change is coincident, but in the longitudinal position of less than 1.0 m or more than 2.1 m, with the increase of the electric field intensity, the pressure drop inside the electric dehydrator increases significantly. While in the longitudinal position of 1.0 ~ 2.1 m, there is no significant difference in the pressure drop, which

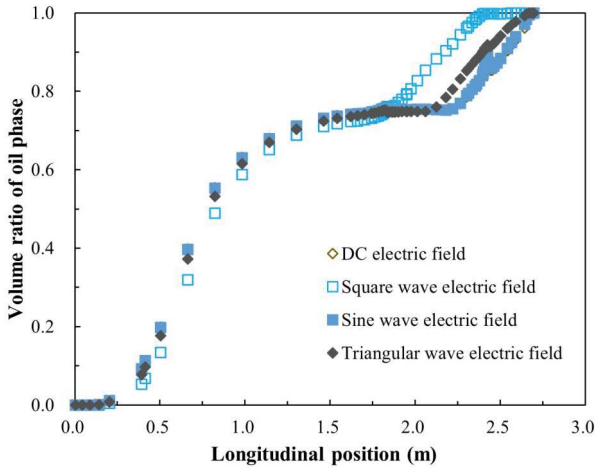

Fig. 9. Proportion of oil phase volume in cross-section of dehydrator under different electric fields.

Table 4
Separation effect of emulsion under different electric fields

Electric field types	Electric field intensity (kV/cm)	Duration time (min)	Current frequency (kHz)	Water content of oil outlet (%)	Separation rate of emulsion (%)
DC	1.5	15	–	2.78	81.47
Square wave			3	1.82	87.87
Sine wave				2.42	83.87
Triangular wave				2.23	85.13

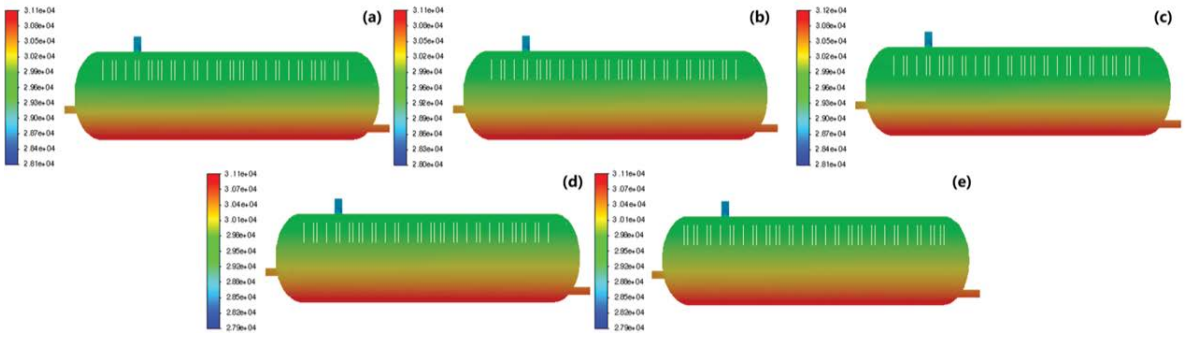

Fig. 10. Internal pressure distribution of dehydrator under electric field intensity with: (a) 0.5 kV/cm, (b) 1.0 kV/cm, (c) 1.5 kV/cm, (d) 2.0 kV/cm and (d) 2.0 kV/cm.

is also consistent with the qualitative description of the pressure field distribution.

3.2.2. Streamline characteristics

As shown in Fig. 12, the flow traces in the electric dehydrator are extracted. when the electric field intensity increases from 0.5 to 2.0 kV/cm, the flow lines between the vertical plates are clear and stable. When the electric field intensity continues to increase to 2.5 kV/cm, there are varying degrees of "Eddy Current" in the electric dehydrator.

3.2.3. Volume fraction of oil phase

The oil–water interface characteristics and oil phase concentration distribution of the dehydrator under different electric field intensities are compared in Fig. 13. The oil–water interface of 0.5 ~ 2.5 kV/cm electric field intensity is relatively flat, and with the increase of electric field intensity, the area of high and low oil phase concentration is significantly thicker and thinner. The proportion of oil phase volume under different electric field intensities is extracted, as shown in Fig. 14. The distribution of oil phase volume proportion in the longitudinal section of the dehydrator is generally regular. The average oil phase volume proportion is the largest when the electric field intensity is 0.5 kV/cm, and it is smaller when the electric field intensity is 2.0 kV/cm. When the longitudinal position is above 1.8 m, the average oil phase volume proportion is the largest when the electric field intensity is 2.0 kV/cm.

3.2.4. Evaluation of oil–water emulsion separation effect

The separation rate of emulsion in dehydrator is calculated by Eq. (8). The separation effect of emulsion under different electric field intensity is shown in Table 5. For emulsion with 15% wat cut, under square wave electric field, when the electric field intensity increases from 0.5 to 2.0 kV/cm, the water content of oil outlet decreases from 2.69% to 1.56%, and the separation rate of emulsion increases from

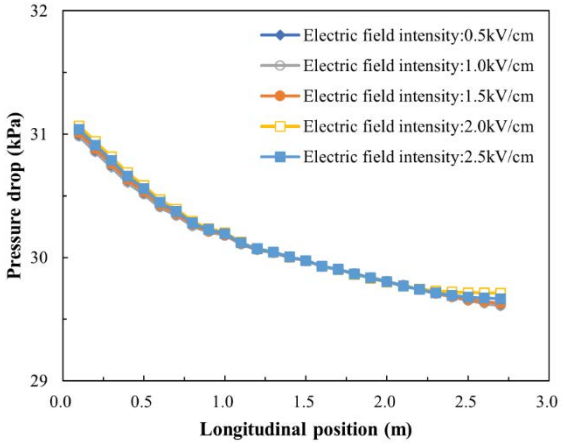

Fig. 11. Cross-sectional pressure drop characteristics of dehydrators with different electric field intensity.

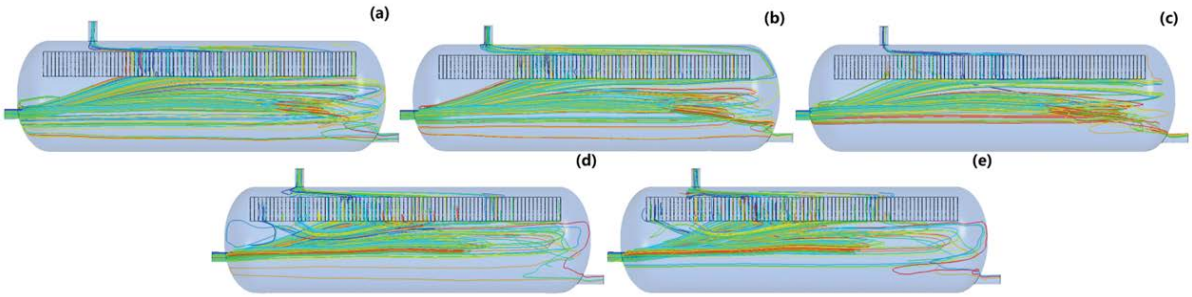

Fig. 12. Internal streamline distribution of dehydrator under electric intensity with: (a) 0.5 kV/cm, (b) 1.0 kV/cm, (c) 1.5 kV/cm, (d) 2.0 kV/cm and (d) 2.0 kV/cm.

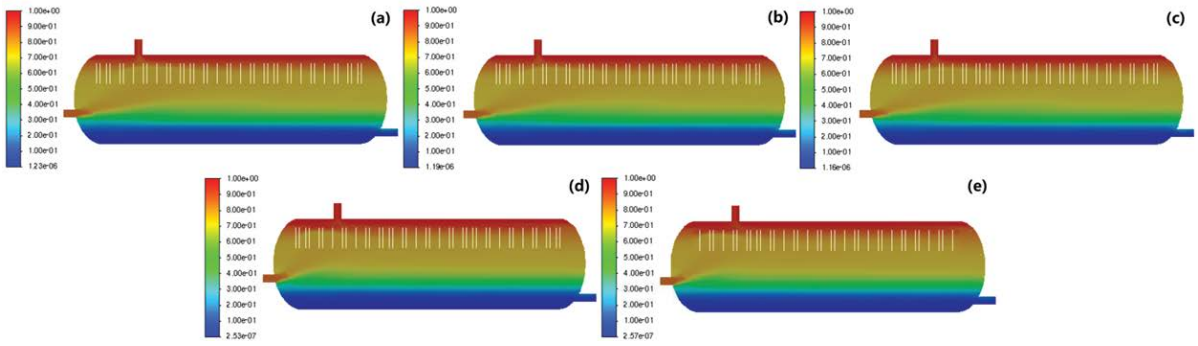

Fig. 13. Distribution of oil phase concentration proportion in dehydrator under electric intensity with: (a) 0.5 kV/cm, (b) 1.0 kV/cm, (c) 1.5 kV/cm, (d) 2.0 kV/cm and (d) 2.0 kV/cm.

82.07% to 89.60%. When the electric field intensity continues to increase from 2.0 to 2.5 kV/cm, the water cut of oil outlet does not change significantly and fluctuates slightly, and the corresponding separation rate of emulsion is also equivalent. Therefore, the distribution characteristics of pressure field, streamline trace and oil phase are considered. The electric field intensity suitable for the coupling effect of electric field and flow field is 2 kV/cm, and the emulsion separation effect is better improved.

3.3. Effect of current frequency

On the basis of the analysis of the effect of electric field type and intensity, the UDF is loaded again. Under the condition of duration time of 15 min and *t* intensity of 1.5 kV/cm, five current frequencies of 1, 2, 3, 4, and 5 kHz are designed. The effect of current frequency change on the electric dehydration effect is simulated and studied.

3.3.1. Pressure field and pressure drop characteristics

As shown in Fig. 15, when the current frequency changes, the internal pressure field distribution of the dehydrator is similar, and the overall pressure field distribution is also relatively stable. However, when the current frequency increases from 1 to 3 kHz, the cross-sectional pressure drop increases significantly. When the current frequency continues to increase to 5 kHz, the increase trend of the cross-sectional pressure drop is not obvious. This can be attributed to the increase of current frequency, the fluctuation and collision of emulsion droplets between electrode plates are intensified, and the settlement and separation of water phase are accelerated, thus showing an increase in cross-sectional pressure drop. As shown in Fig. 16, the pressure drop characteristic curve drawn by the average pressure drop. When the longitudinal position is below 1.0 m or above 2.1 m, the internal pressure drop of the dehydrator increases with the increase of the current frequency. When the longitudinal position is between 1.0 and 2.1 m, the internal pressure drop has no obvious difference.

3.3.2. Streamline characteristics

The streamline in the dehydrator is shown in Fig. 17. With the increase of the current frequency, the collision, coalescence, and separation of the emulsion droplets between the electrode plates are strengthened, which is beneficial

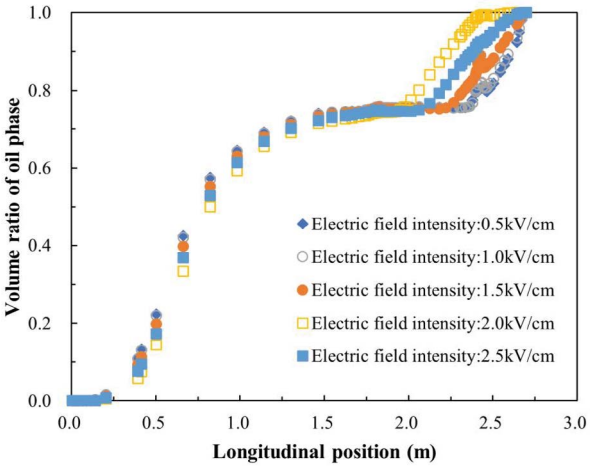

Fig. 14. Proportion of oil phase volume in cross-section of dehydrator under different electric intensity.

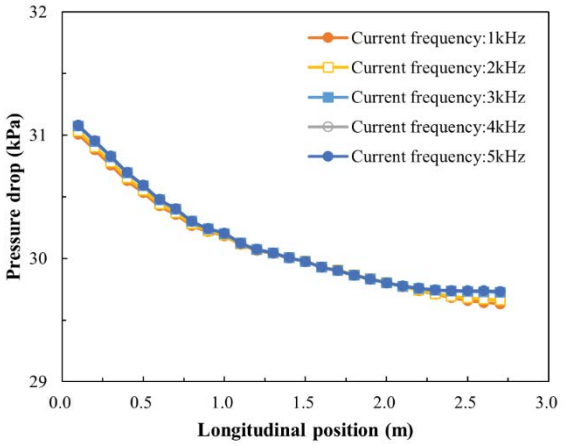

Fig. 16. Cross-sectional pressure drop characteristics of dehydrators with different current frequency.

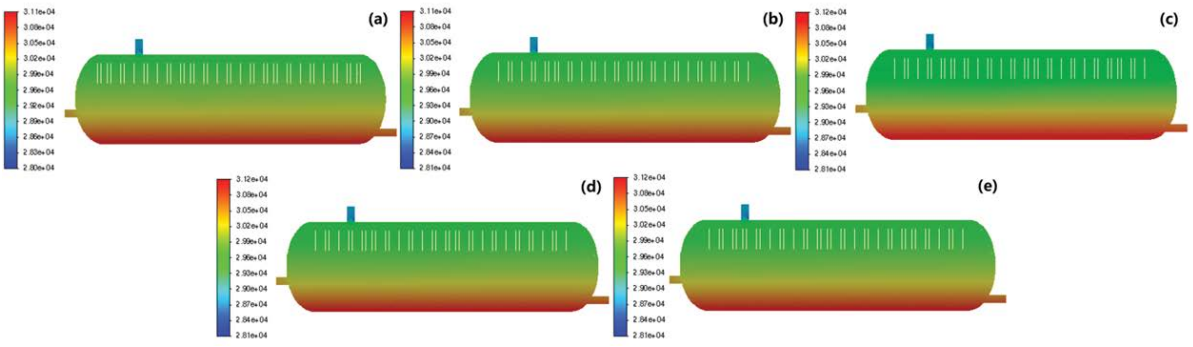

Fig. 15. Internal pressure distribution of dehydrator under current frequency with: (a) 1 kHz, (b) 2 kHz, (c) 3 kHz, (d) 4 kHz and (d) 5 kHz.

Table 5
Separation effect of emulsion under different electric intensity

Electric field types	Electric field intensity (kV/cm)	Duration time (min)	Current frequency (kHz)	Water content of oil outlet (%)	Separation rate of emulsion (%)
Square wave	0.5	15	3	2.69	82.07
	1.0			2.16	85.60
	1.5			1.82	87.87
	2.0			1.56	89.60
	2.5			1.58	89.47

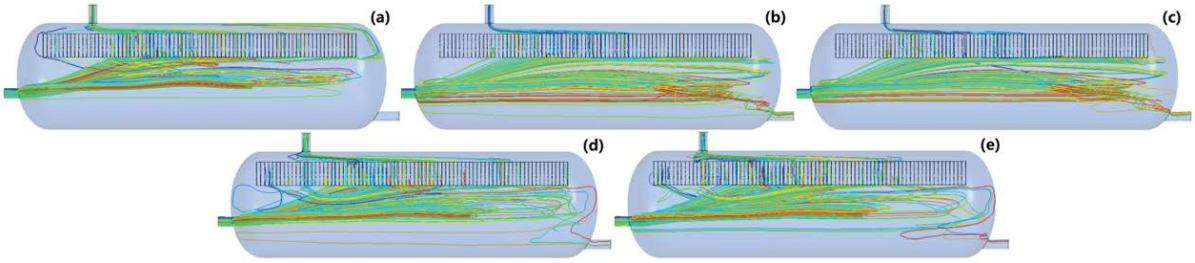

Fig. 17. Internal streamline distribution of dehydrator under current frequency with: (a) 1 kHz, (b) 2 kHz, (c) 3 kHz, (d) 4 kHz and (d) 5 kHz.

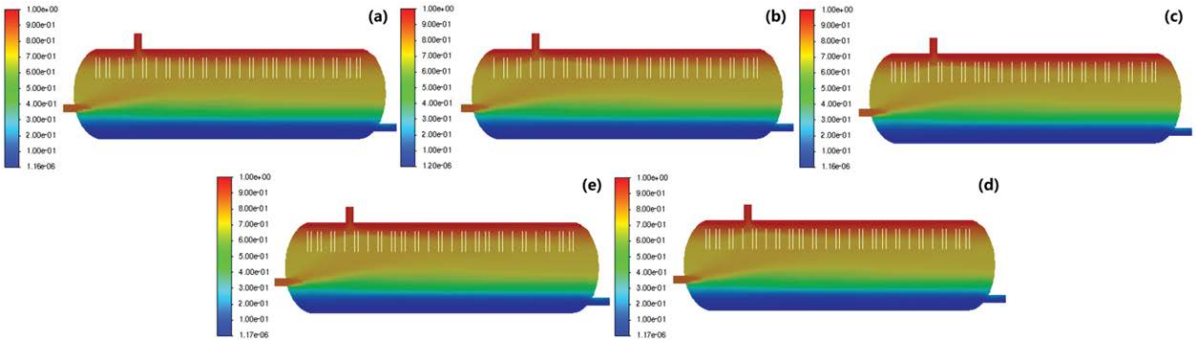

Fig. 18. Distribution of oil phase concentration proportion in dehydrator under current frequency with: (a) 1 kHz, (b) 2 kHz, (c) 3 kHz, (d) 4 kHz and (d) 5 kHz.

to provide a stable flow field for the dehydrator chamber. However, when the current frequency exceeds 3 kHz, the movement of the emulsion droplets is too intense and continues to propagate, which makes the streamline in the dehydrator chamber more disordered, and thus the stability of the internal flow field is affected.

3.3.3. Volume fraction of oil phase

It can be seen from Fig. 18 that after the square wave electric field is introduced into the separation flow field, the current frequency is increased, and the area of higher oil phase transition thickness and lower oil phase concentration in the dehydrator become thinner. When the current frequency reaches 3 kHz, the area of high oil phase and low oil phase concentration reaches the extreme value, and then the current frequency is increased, and the change of oil–water interface is no longer obvious. As shown in Fig. 19, the proportion of oil phase volume under different current frequencies is extracted. The distribution of oil phase volume proportion in the longitudinal section of the electric dehydrator is relatively regular. When the longitudinal position is below 1.8 m, the average oil phase volume proportion is larger at the current frequency of 1 kHz and smaller at 3 kHz. When the longitudinal position is above 1.8 m, the average oil phase volume proportion is the largest at the current frequency of 3 kHz. In the frequency range of 3 to 5 kHz, the average oil phase volume proportion is almost coincident.

3.3.4. Evaluation of oil–water emulsion separation effect

The separation rate of emulsion under different current frequencies is calculated by Eq. (8), as shown in Table 6. When the current frequency increases from 1 to 3 kHz, the water content at the oil outlet decreases from 2.46% to 1.82%. Accordingly, the separation rate of emulsion

increases from 83.60% to 87.87%. Then, when the current frequency increases from 3 to 5 kHz again, the water content at the oil outlet increases from 1.82% to 1.90%, and the corresponding separation rate of emulsion decreases from 87.87% to 87.33%. Therefore, the separation effect under the coupling of separation flow field and electric field is qualitatively described. The appropriate current frequency is determined to be 3 kHz.

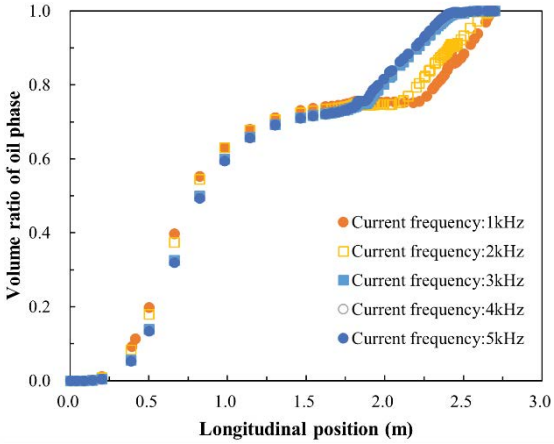

Fig. 19. Proportion of oil phase volume in cross-section of dehydrator under different current frequency.

3.4. Effect of duration time

After the electric field condition is studied, the duration time of the oil–water emulsion in the electric dehydration process is further simulated in order to better observe the coupling effect of the flow field and electric field at different times. When the square wave electric field intensity is 1.5 kV/cm and the current frequency is 3 kHz, four duration time of 10, 15, 20 and 25 min are selected to simulate.

3.4.1. Pressure field and pressure drop characteristics

As shown in Fig. 20, for different operation schemes, the internal pressure field distribution of the dehydrator is generally more regular, but the duration time is prolonged, and the cross-sectional pressure drop is significantly increased, which is mainly due to the extension of the duration time. At the same time, the flow rate of the incoming liquid equivalent to the inlet of the electric dehydrator is reduced, the amount of the incoming liquid is reduced and the pressure loss is reduced. The cross-sectional pressure drop of the electric dehydrator is further extracted to draw Fig. 21. The figure shows that when the longitudinal position is less than 1.0 m or more than 2.1 m, the internal pressure drop of

Table 6
Separation effect of emulsion under different current frequency

Electric field types	Electric field intensity (kV/cm)	Duration time (min)	Current frequency (kHz)	Water content of oil outlet (%)	Separation rate of emulsion (%)
Square wave	1.5	15	1	2.46	83.60
			2	2.26	84.93
			3	1.82	87.87
			4	1.87	87.53
			5	1.90	87.33

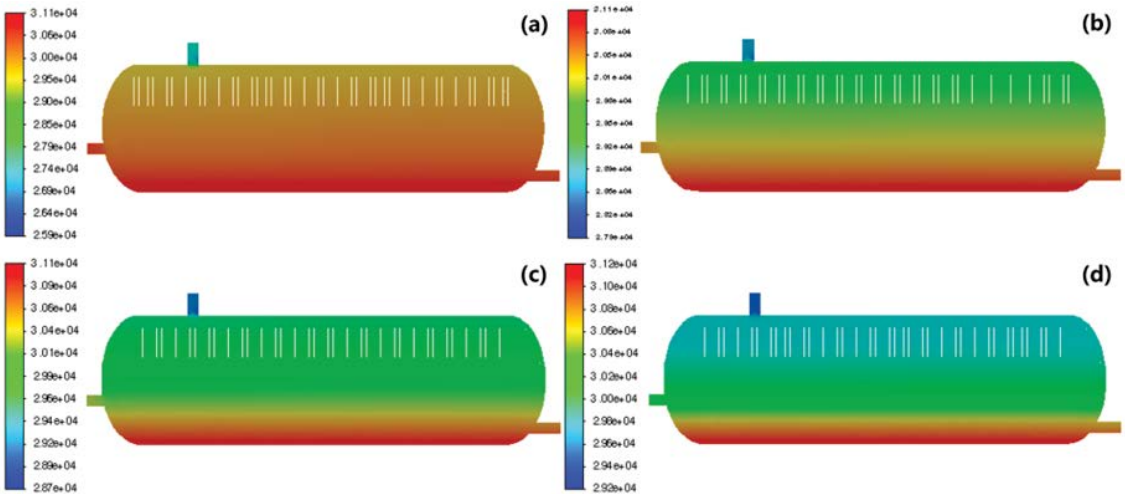

Fig. 20 Internal pressure distribution of dehydrator under duration time with: (a) 10 min, (b) 15 min, (c) 320 min and (d) 25 min.

the dehydrator increases slightly with the extension of the duration time. When the longitudinal position is between 1.0 and 2.1 m, there is no obvious difference in the internal pressure drop, which is consistent with the qualitative description of the pressure distribution.

3.4.2. Streamline characteristics

Fig. 22 shows the flow distribution inside the dehydrator in the simulated operation scenario. By comparison, it can be seen that the eddy current phenomenon in Fig. 22a gradually disappears with increasing duration time, indicating that the separation stability is increasing and the separation of emulsions will be improved.

3.4.3. Volume fraction of oil phase

Fig. 23 shows the distribution of the oil phase concentration in the electric dehydrator for different durations. The duration time is prolonged, the distribution area of high oil phase concentration is significantly thicker, and the distribution area of low oil phase concentration is significantly thinner, which is consistent with the actual situation. As shown in Fig. 24, the distribution of oil phase volume proportion in the longitudinal section of the dehydrator is relatively regular. When the longitudinal position is below 1.8 m, the average oil phase volume proportion is the largest at the duration time of 10 min and the smallest at the

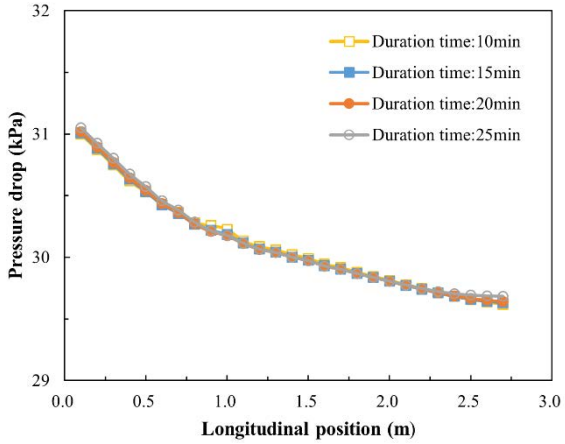

Fig. 21. Cross-sectional pressure drop characteristics of dehydrators with different duration time.

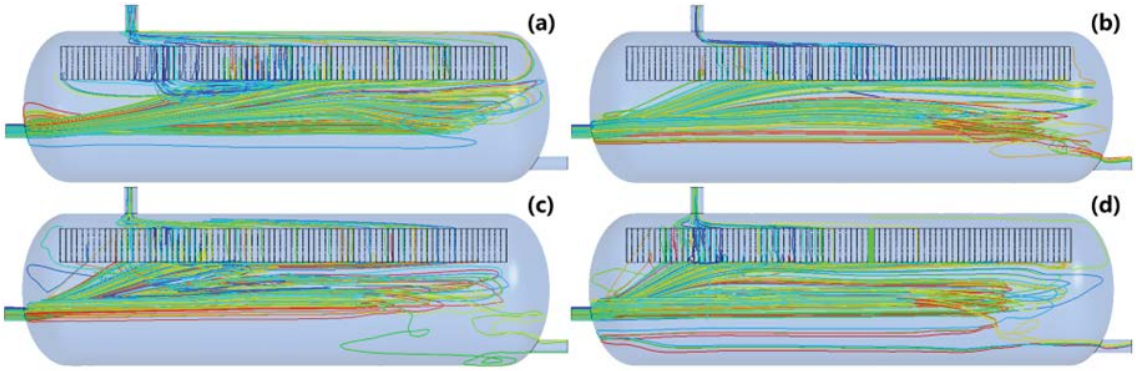

Fig. 22. Internal streamline distribution of dehydrator under duration time with: (a) 10 min, (b) 15 min, (c) 320 min and (d) 25 min.

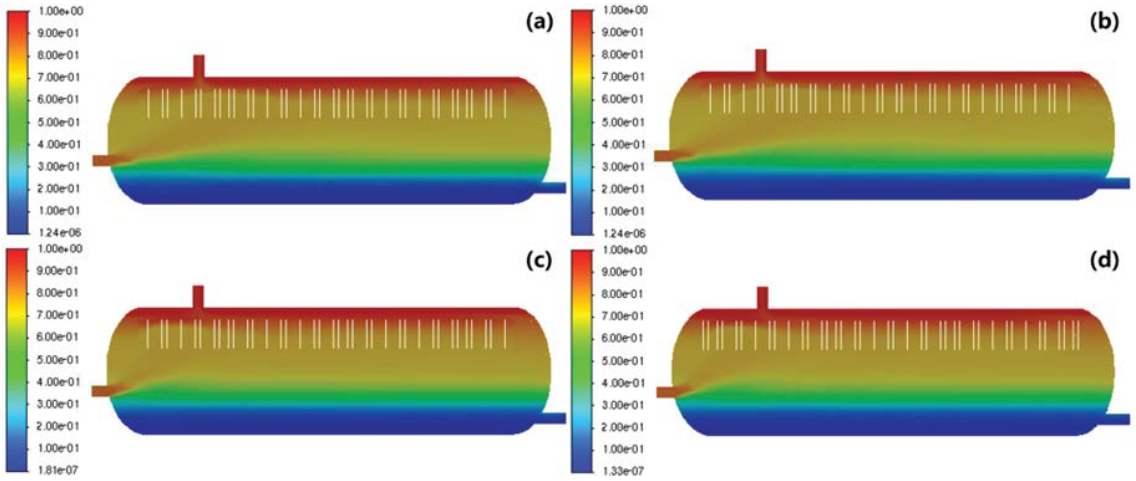

Fig. 23. Distribution of oil phase concentration proportion in dehydrator under duration time with: (a) 10 min, (b) 15 min, (c) 320 min and (d) 25 min.

duration time of 25 min. When the longitudinal position is above 1.8 m, the average oil phase volume proportion is the largest at the duration time of 25 min and the smallest at the duration time of 10 min.

3.4.4. Evaluation of oil–water emulsion separation effect

Table 7 shows the separation effect of emulsion under different duration time. When the duration time is prolonged, the separation effect of emulsion is improved. When the duration time is prolonged from 10 min to 25 min, the water content at the oil outlet is reduced from 2.77% to 1.26%, and the corresponding separation rate of emulsion is increased from 81.53% to 91.60%, which is increased by nearly 10%. Among them, when the duration time is increased from 10 to 15 min, the increase of the separation rate of emulsion reached the maximum value of 6.34%. After that, when the duration time is prolonged, the increase of the separation rate of emulsion is further reduced. It is concluded that the duration time suitable for the coupling effect of square wave electric field and separation flow field is 20 min, and the separation effect of emulsion can be guaranteed.

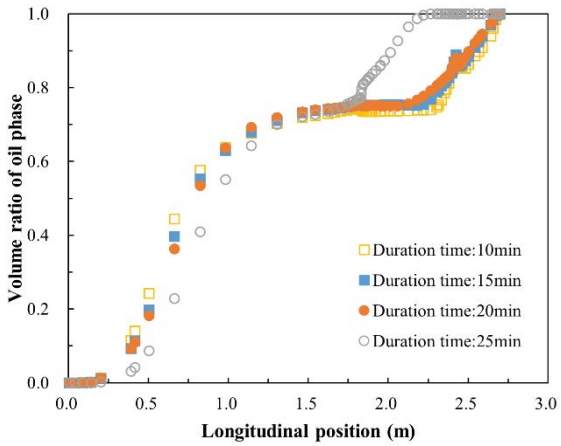

Fig. 24. Proportion of oil phase volume in cross-section of dehydrator under different duration time.

3.5. Validation of numerical simulation

The electric field dehydration experiment of oil–water emulsion can be evaluated from two aspects. One is the dehydration effect, obtaining the "water content in oil" and "oil content in water" after dehydration. The other is to construct the stability of the electric field, which can be determined by the peak current and current changes in the dehydration process. After the oil–water emulsion with three moisture content is prepared, the experimental design is carried out, and the dehydration of emulsion bottles under different electric field is obtained. As shown in Fig. 25, the dehydration performance of square wave electric field is better than that of DC electric field.

3.5.1. DC electric field

For the DC electric field, the dehydration experiment results are shown in Fig. 26. When the electric field intensity is 2.0 kV/cm and the duration time is about 15 min, the water content of purified oil does not exceed 0.5% and the oil content of sewage does not exceed 60 mg/L. The change of dehydration current reflects that the peak current of dehydration in the experiment is about 800 mA, and the time to maintain the dehydration current near the peak is about 6 min. During the experiment, the phenomenon of "Cross-Electric Field" occurs occasionally. After the duration time of different liquid systems exceeds 15 min, the dehydration current drops to zero.

3.5.2. Square wave electric field

The experimental results of square wave electric field dehydration are shown in Fig. 27. When the electric field

Table 7
Separation effect of emulsion under different duration time

Electric field types	Electric field intensity (kV/cm)	Duration time (min)	Current frequency (kHz)	Water content of oil outlet (%)	Separation rate of emulsion (%)
Square wave	1.5	10	3	2.77	81.53
		15		1.82	87.87
		20		1.41	90.60
		25		1.26	91.60

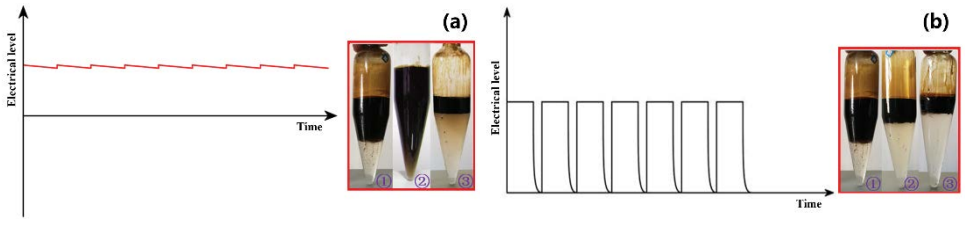

Fig. 25. Experiment of bottle dehydration under electric field with (a) DC and (b) square wave.

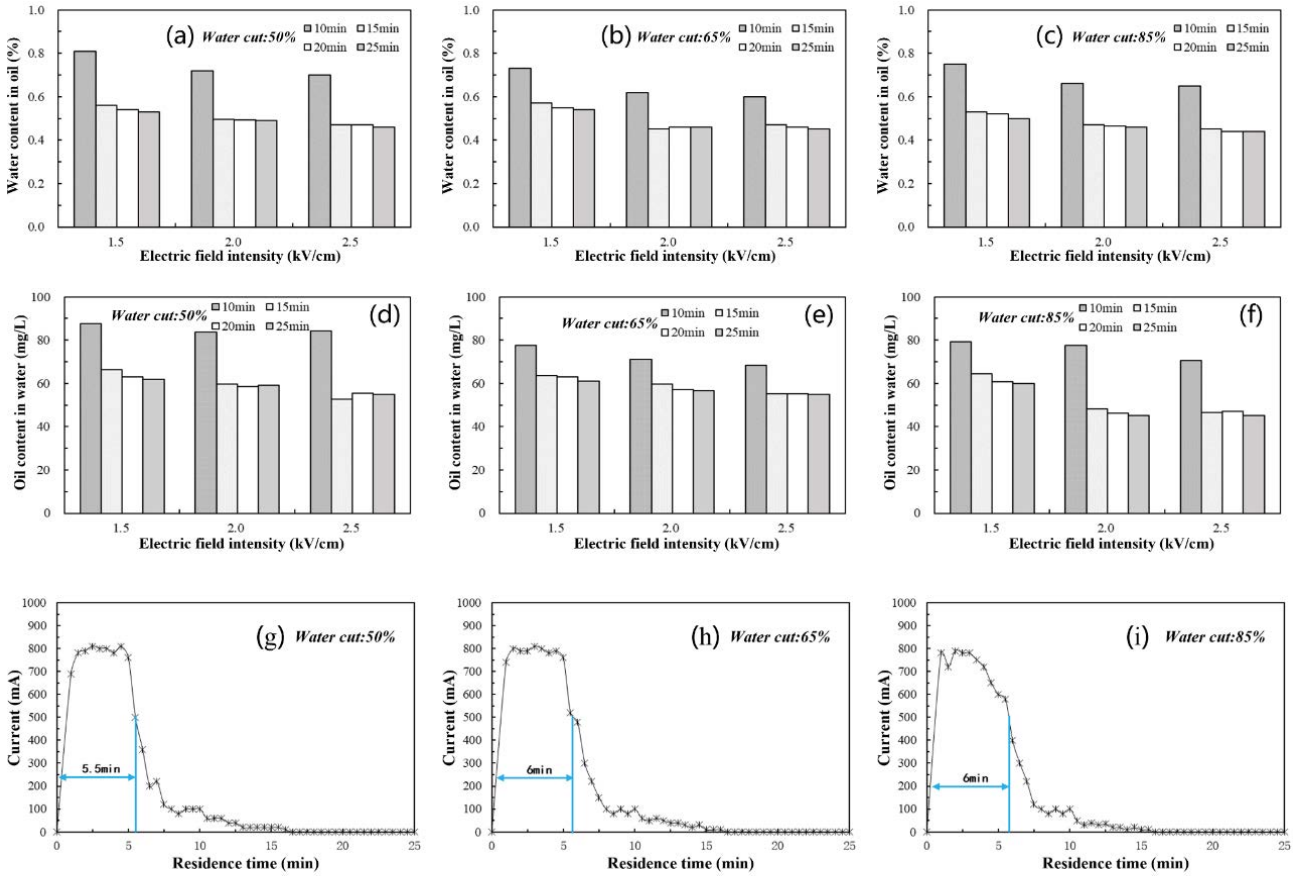

Fig. 26. Experimental results of DC electric field dehydration. Water contents in oil are shown in (a–c); oil contents in water are shown in (d–f); dehydration current are shown in (g–i).

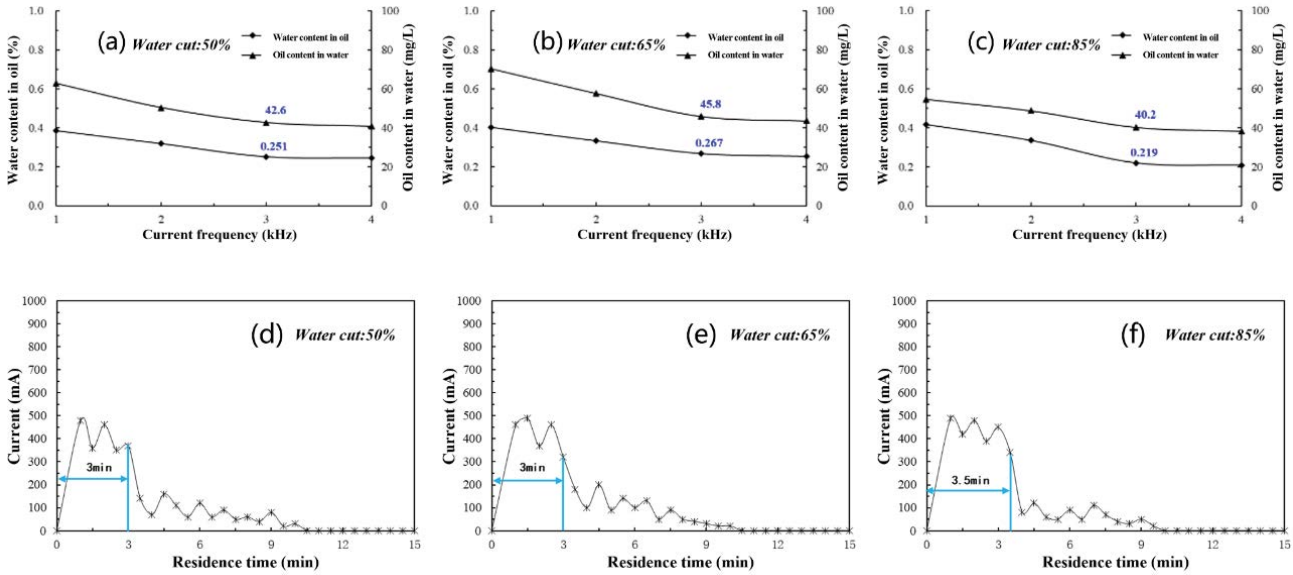

Fig. 27. Experimental results of square wave electric field dehydration. Water contents in oil and oil contents in water are shown in (a–c); dehydration current are shown in (d–f).

intensity is 2.0 kV/cm and the duration time is 15 min, the current frequency of 3 kHz, the water content of less than 0.3% of the purified oil and the oil content of 50 mg/L of the sewage are obtained. The current frequency continues to increase, and the improvement of dehydration effect tends to be stable. At 4 kHz, the decrease of "Water Content In Oil" and "Oil Content in Water" is less than 5% compared with that at 3 kHz. Under the condition of square wave electric field, although the change of dehydration current reflects the large fluctuation of current, the dehydration current value is low as a whole. The dehydration peak current of the experimental emulsion is not more than 500 mA, and the time to maintain the peak dehydration current is only within 3 min, which is about half of the time to maintain the peak dehydration current under DC electric field. It reveals that the stable emulsion dehydration process under square wave electric field, and the fluctuation current decreases to zero after the duration time of about 10 min.

After dehydration, the oil–water emulsion separation experiment met the requirements of water content of purified oil lower than 1.0% and oil content in water lower than 1,000 mg/L. According to the above experimental results, the dehydration performance of square wave electric field is better. It has the best separation effect when the electric field intensity is 2.0 kV/cm, the duration time is 15 min and the current frequency is 3 kHz. This is in general agreement with the results of the numerical simulations, which are confirmed by the experimental study.

4. Conclusions

The study is realized by writing UDF for the construction of different electric field types and loading them into FLUENT software. Thus, a numerical simulation of electric field dehydration process is achieved. Furthermore, the coupling effect of separation flow field and electric field is considered, the pressure field, streamline and oil phase volume ratio distribution inside the electric dehydrator are described, and the characteristics and influence of electric field separation process of oil–water emulsion are revealed.

The emulsified water droplets will accelerate the agglomeration and settlement under the action of electric field force, which is most obvious in the area near the electrode plate. The electric field action increases the pressure drop inside the separator and forms a stable pressure field, and the regularly distributed pressure field can ensure the effect of oil–water separation. The streamline further demonstrate that the introduction of electric field can avoid the turbulence of the flow field, and the smooth flow line means that the electric field can provide a more stable separation flow field environment. In addition, a stable flow field interacting with the electric field can obtain a smoother oil–water interface. By varying the electric field strength and frequency, it is found that the electric field action is not always positive, while too high electric field action will cause the oil–water separation effect to decrease, and there is a threshold value of electric field action. After quantitative analysis of oil–water separation efficiency, a stable flow field and suitable duration will increase the gain of electric field action and bring better separation performance.

After simulation and verification, the optimal operation parameters of electric field dehydration are obtained: square wave, electric field intensity of 2.0 kV/cm, current frequency of about 3 kHz, and duration time of about 20 min. The optimized parameters are used to make the water content of oil outlet less than 1.5% and the separation rate of emulsion higher than 90%.

Acknowledgements

This work presented in this paper was financially supported by the National Natural Science Foundation of China (Grant No. 52174060; 52074090). The authors also gratefully acknowledge the support from the Heilongjiang Touyan Innovation Team Program.

Appendix

A1. DC electric field

Taking the DC field with electric field intensity of 1.5 kV/cm as an example, the UDF function is as follows:

```
#include "udf.h"

#define RO 0.02

DEFINE_SOURCE (xmom_source_secondphase, c, t,
dS, eqn)

{

real v;

real time = RP_Get_Real("flow-time");

v = 13500;

real source;

source = v * C_VOF(c, t) * RO;

C_UDMI(c,t,0) = source;

dS[eqn] = 0;

return source;

}
```

A2. Square wave electric field

Taking the square wave field with electric field intensity of 1.5 kV/cm and current frequency of 3 kHz as an example, the UDF function is as follows:

```
#include "udf.h"

#define RO 0.02

DEFINE_SOURCE (xmom_source_secondphase, c, t,
dS, eqn)

{

real v;
```

```
real time = RP_Get_Real("flow-time");

real T = 0.003;

int a;

real b;

a = (int)(time / T);

b = time – T * a;

if (b <= T/2)

v = 13500;

else

v = 0;

real source;

source = v * C_VOF(c, t) * RO;

C_UDMI(c,t,0) = source;

dS[eqn] = 0;

return source;

}
```

A3. Sine wave electric field

Taking the sine wave field with electric field intensity of 1.5 kV/cm and current frequency of 3 kHz as an example, the UDF function is as follows:

```
#include "udf.h"

#define RO 0.02

DEFINE_SOURCE (xmom_source_secondphase, c, t, dS,
eqn)

{

real v;

real time = RP_Get_Real("flow-time");

real T = 0.003;

v = 13,500 * sin(2 * 3.1415926 * 1.0/T * time) + 13,500;

real source;

source = v * C_VOF(c, t) * RO;

C_UDMI(c, t, 0) = source;

dS [eqn] = 0;

return source;

}
```

A4. Triangular wave electric field

Taking the triangular wave field with electric field intensity of 1.5 kV/cm and current frequency of 3 kHz as an example, the UDF function is as follows:

```
#include "udf.h"

#define RO 0.02

DEFINE_SOURCE (xmom_source_secondphase, c, t, dS,
eqn)

{

real v;

real time = RP_Get_Real("flow-time");

real T = 0.003;

int a;

real b;

a = (int)(time / T);

b = time – T * a;

if (b <= T/2)

v = 2 * 13,500/T * b;

else

v = –2 * 13500/T * b+2 * 13,500;

real source;

source = v * C_VOF(c, t) * RO;

C_UDMI(c, t, 0) = source;

dS[eqn] = 0;

return source;

}
```

References

[1] X. Zhang, L. Zhao, J. Wang, L. Chen, X. Yue, Residual Oil Distribution of Heterogeneous Reservoir at Different Water Drive Velocity, Proceedings of the International Field Exploration and Development Conference 2017, Springer, Singapore, 2019.

[2] D. Wijeratne, B.M. Halvorsen, Computational study of fingering phenomenon in heavy oil reservoir with water drive, Fuel, 158 (2015) 306–314.

[3] Z. Wang, Y. Xu, Y. Gan, X. Han, W. Liu, H. Xin, Micromechanism of partially hydrolyzed polyacrylamide molecule agglomeration morphology and its impact on the stability of crude oil–water interfacial film, J. Pet. Sci. Eng., 214 (2022) 110492, doi: 10.1016/j.petrol.2022.110492.

[4] D. Ramirez, C.D. Collins, Maximisation of oil recovery from an oil–water separator sludge: influence of type, concentration, and application ratio of surfactants, Waste Manage., 82 (2018) 100–110.

[5] H. Zhong, Y. He, E. Yang, Y. Bi, T. Yang, Modeling of microflow during viscoelastic polymer flooding in heterogenous reservoirs of Daqing Oilfield, J. Pet. Sci. Eng., 210 (2022) 110091, doi: 10.1016/j.petrol.2021.110091.
[6] Q. Gao, Y. Wang, Y. Jiang, Study on scaling formation characteristics and produced liquid properties in oil–wells of ASP Flooding, Adv. Mater. Res., 524 (2012) 1270–1278.
[7] Y.V. Savinykh, D.I. Chuykina, L.D. Stakhina, Impact of integrated technologies of enhanced oil recovery on the changes in the composition of heavy oil, J. Sib. Fed. Univ.: Chem., 13 (2020) 17–24.
[8] U.A. Aziz, N. Adnan, M.Z.R. Sohri, D.F. Mohshim, A.K. Idris, M.A. Azman, Characterization of anionic–nonionic surfactant mixtures for enhanced oil recovery, J. Solution Chem., 48 (2019) 1617–1637.
[9] Z.-H. Wang, X.-Y. Liu, H.-Q. Zhang, Y. Wang, Y.-F. Xu, B.-L. Peng, Y. Liu, Modeling of kinetic characteristics of alkaline-surfactant-polymer-strengthened foams decay under ultrasonic standing wave, Pet. Sci., 19 (2022) 1825–1839.
[10] H. Liu, G. Jia, S. Chen, Y. Cai, Optimization of flow deflector quantities for gravity oil–water separator, Appl. Mech. Mater., 675 (2014) 685–688.
[11] H. Luo, J. Wen, C. Lv, Z. Wang, Modeling of viscosity of unstable crude oil–water mixture by characterization of energy consumption and crude oil physical properties, J. Pet. Sci. Eng., 212 (2022) 110222, doi: 10.1016/j.petrol.2022.110222.
[12] D.D. Fazullin, L.I. Fazullina, D.A. Yarovikova, G.V. Mavrin, I.A. Nasyrov, I.G. Shaikhiev, Demulsification and ultrafiltration of water-oil emulsions, Chem. Pet. Eng., 57 (2022) 783–791.
[13] D. Langevin, J.F. Argillier, Interfacial behavior of asphaltenes, Adv. Colloid Interface Sci., 233 (2016) 222–227.
[14] A.M. Sousa, M.J. Pereira, H.A. Matos, Oil-in-water and water-in-oil emulsions formation and demulsification, J. Pet. Sci. Eng., 210 (2022) 110041, doi: 10.1016/j.petrol.2021.110041.
[15] Y. Dhandhi, R.K. Chaudhari, T.K. Naiya, Development in separation of oilfield emulsion toward green technology – a comprehensive review, Sep. Sci. Technol., 57 (2021) 1642–1668.
[16] H. Pramadika, A.R. Wastu, B. Satiyawira, C. Rosyidan, M. Maulani, A. Prima, L. Samura, Z. Darajat, Demulsification optimization process on separation of water with heavy oil, AIP Conf. Proc., 2363 (2021) 020029, doi: 10.1063/5.0061527.
[17] H. Gong, W. Li, X. Zhang, Y. Peng, B. Yu, Y. Mou, Simulation of the coalescence and breakup of water-in-oil emulsion in a separation device strengthened by coupling electric and swirling centrifugal fields, Sep. Purif. Technol., 238 (2020) 116397, doi: 10.1016/j.seppur.2019.116397.
[18] N.H. Abdurahman, R.B. Yunus, N.H. Azhari, N. Said, Z. Hassan, The potential of microwave heating in separating water-in-oil (w/o) emulsions, Energy Procedia, 138 (2017) 1023–1028.
[19] S.A. Solovyev, O.V. Solovyeva, R.R. Yafizov, S.I. Ponikarov, I.Y. Portnov, Study of the influence of coalescence baffle inclination angle on the intensity of water-oil emulsion separation in a separator section, Chem. Pet. Eng., 57 (2021) 19–24.
[20] C. Atehortúa, N. Pérez, M. Andrade, L. Pereira, J.C. Adamowski, Water-in-oil emulsions separation using an ultrasonic standing wave coalescence chamber, Ultrason. Sonochem., 57 (2019) 57–61.
[21] X. Li, L. Han, Z. Huang, Z. Li, F. Li, H. Duan, L. Huang, Q. Jia, H. Zhang, S. Zhang, A robust air superhydrophilic/superoleophobic diatomite porous ceramic for high-performance continuous separation of oil-in-water emulsion, Chemosphere, 303 (2022) 134756, doi: 10.1016/j.chemosphere.2022.134756.
[22] F. Li, X. Wan, J. Hong, X. Guo, M. Sun, H. Lv, H. Wang, J. Mi, J. Cheng, X. Pan, M. Xu, Z. Wang, A self-powered and efficient triboelectric dehydrator for separating water-in-oil emulsions with ultrahigh moisture content, Adv. Mater. Technol., 7 (2022) 2200198, doi: 10.1002/admt.202200198.
[23] B. Ren, Y. Kang, Aggregation of oil droplets and demulsification performance of oil-in-water emulsion in bidirectional pulsed electric field, Sep. Purif. Technol., 211 (2019) 958–965.
[24] F. Esmaelion, H. Tavanai, A.A.M. Beigi, M. Bazarganipour, Application of fibrous structures in separation of water and oil emulsions: a review, J. Environ. Chem. Eng., 10 (2022) 107999, doi: 10.1016/j.jece.2022.107999.
[25] B. Xu, Fast and energy-efficient demulsification for crude oil emulsions using pulsed electric field, Int. J. Electrochem. Sci., 12 (2017) 9242–9249.
[26] K. Guo, Y. Lv, L. He, X. Luo, D. Yang, Separation characteristics of w/o emulsion under the coupling of electric field and magnetic field, Energy Fuel, 33 (2019) 2565–2574.
[27] S. Mhatre, S. Simon, J. Sjöblom, Z. Xu, Demulsifier assisted film thinning and coalescence in crude oil emulsions under dc electric fields, Chem. Eng. Res. Des., 134 (2018) 117–129.
[28] M. Mohammadi, S. Shahhosseini, M. Bayat, Direct numerical simulation of water droplet coalescence in the oil, Int. J. Heat Fluid Flow, 36 (2012) 58–71.
[29] F.M. Fowkes, F.W. Anderson, J.E. Berger, Bimetallic coalescers: electrophoretic coalescence of emulsions in beds of mixed-metal granules, Environ. Sci. Technol., 4 (2002) 510–514.
[30] Y. Peng, L. Tao, H. Gong, X. Zhang, Review of the dynamics of coalescence and demulsification by high-voltage pulsed electric fields, Int. J. Chem. Eng., 4 (2016) 1–8.
[31] K. Adamiak, J.M. Floryan, Dynamics of Water Droplet Distortion and Break-Up in a Uniform Electric Field, 2010 IEEE Industry Applications Society Annual Meeting, IEEE, Houston, TX, USA, 2010, pp. 2374–2383.
[32] S.H. Mousavi, M. Ghadiri, M. Buckley, Electro-coalescence of water drops in oils under pulsatile electric fields, Chem. Eng. Sci., 120 (2014) 130–142.
[33] S. Ervik, S.M. Helles, S.T. Munkejord, B. Müller, Experimental and Computational Studies of Water Drops Falling Through Model Oil with Surfactant and Subjected to an Electric Field, 2014 IEEE 18th International Conference on Dielectric Liquids (ICDL), IEEE, Bled, Slovenia, 2014.
[34] Z. Wang, X. Le, Y. Feng, Z. Hu, Dehydration of aging oil by an electrochemical method, Chem. Technol. Fuels Oils, 50 (2014) 262–268.
[35] Y. Song, Y. Xu, Z. Wang, An experimental study on efficient demulsification for produced emulsion in alkaline/surfactant/polymer flooding, J. Energy Resour. Technol., 144 (2022) 093001, doi: 10.1115/1.4053136.
[36] N. Koutsourakis, J.G. Bartzisa, N.C. Markatos, Evaluation of Reynolds stress, k–ε and RNG k–ε turbulence models in street canyon flows using various experimental datasets, Environ. Fluid Mech., 12 (2012) 379–403.
[37] Y. Mori, M. Sakai, Development of a robust Eulerian–Lagrangian model for the simulation of an industrial solid–fluid system, Chem. Eng. J., 406 (2021) 126841, doi: 10.1016/j.cej.2020.126841.
[38] R. Keser, V. Vukčević, M. Battistoni, H.G. Im, H. Jasak, Implicitly coupled phase fraction equations for the Eulerian multi-fluid model, Comput. Fluids, 192 (2019) 104277, doi: 10.1016/j.compfluid.2019.104277.
[39] D.C. Wilcox, Turbulence Modeling for CFD, DCW Industries, 2006.
[40] T.K. Bandyopadhyay, CFD Analysis for Non-Newtonian and Gas-Non-Newtonian Liquid Flow, LAP LAMBERT Academic Publishing, Saarbrucken, 2013.